

Fundamental parameters of bright Ap stars from wide-range energy distributions and advanced atmospheric models

D. Shulyak¹, T. Ryabchikova^{2,3}, and O. Kochukhov⁴

¹ Institute of Astrophysics, Georg-August University, Friedrich-Hund-Platz 1, D-37077 Göttingen, Germany

² Institute of Astronomy, Russian Academy of Science, Pyatnitskaya 48, 119017 Moscow, Russia

³ Universität Wien, Institut für Astronomie, Türkenschanzstraße 17, 1180 Wien, Austria

⁴ Department of Physics and Astronomy, Uppsala University, Box 516, 751 20, Uppsala, Sweden

Received / Accepted

ABSTRACT

Aims. The determination of atmospheric and stellar parameters, being a well established procedure for the vast majority of normal main-sequence stars, turns to be a challenging process in case of magnetic chemically peculiar stars. Inhomogeneous distribution of chemical elements and presence of strong magnetic fields make most of the standard photometric and spectroscopic calibrations inapplicable for this class of stars. In this work we make use of available observed energy distributions calibrated to absolute units, stellar parallaxes, high-resolution spectroscopic observations, and advanced stellar atmosphere models to derive parameters of three bright Ap stars: 33 Lib, γ Equ, and β CrB.

Methods. Model atmospheres and fluxes were computed employing LLMODELS code. SYNTH3 and SYNTHMAG codes were used to compute profiles of individual spectral lines involved in abundance analysis.

Results. For each of the star we construct a self-consistent atmospheric models assuming normal and depleted helium compositions and derive empirically stratification profiles of certain elements. The effective temperatures and surface gravities are found from the simultaneous fit to spectroscopic, photometric, and spectrophotometric observations calibrated to absolute units. We show that using advanced model atmospheres and accurate stellar parallaxes allows one to derive stellar radii with high accuracy and which are consistent with those obtained from independent but more complicated interferometric observations.

Key words. stars: chemically peculiar – stars: atmospheres – stars: abundances – stars: fundamental parameters – stars: individual: HD 137909, HD 137949, HD 201601

1. Introduction

The accurate knowledge of fundamental stellar (mass, radius, luminosity, metallicity, age) and atmospheric (effective temperature, surface gravity, atmospheric abundances) parameters is essential for many fields of modern astrophysics. Stellar masses and abundances determine the whole chain of stellar evolution stages of a single star, and obtaining stellar luminosities and radii by means of observed data allows one to determine ages of stars as well as derive other parameters of interest, such as atmospheric chemistry from spectroscopic observations, characterise extrasolar planets from transit data, carry out asteroseismic modelling, and many more.

The determination of stellar parameters is a delicate process even in case of normal stars because it relies on theoretical evolutionary and atmospheric models. The former requires the knowledge of metallicities and masses, the latter also needs effective temperatures and gravities as inputs. These are usually obtained from spectroscopic and photometric data employing well-developed calibration schemes. In case of Chemically Peculiar (CP) stars, however, things get much more complicated mainly because of abnormal chemical composition of their atmospheres (see, e.g., Ryabchikova et al. 2004). This makes the spectra and energy distributions of CP stars look much different from their normal analogs and therefore most of the photometric calibrations simply fail to work for CP stars. Furthermore, a

presence of strong surface magnetic fields detected in many CP stars adds additional complication to the analysis of their spectra and determination of atmospheric parameters.

Since all parameters are linked together, the accuracy in such derived parameters as, e.g., T_{eff} and $\log(g)$ must be as high as possible. This is why the full set of stellar and atmospheric parameters ideally can only be derived using iterative procedure where each parameter is adjusted in such a way to fit all available observed data. Then, if needed, the other parameters are re-calculated accordingly. For instance, deriving T_{eff} and $\log(g)$ from photometric data and employing relevant calibrations one can carry out a detailed abundance analysis based on model atmospheres, but if derived abundances turn out to be different from those assumed in the construction of the model atmospheres then the later must be recalculated with appropriate chemistry and the whole process should be repeated again. Because of the lack of appropriate calibrations and the large diversity of abundance patterns, this is the only robust scheme for the analysis of CP stars (see, e.g., Kochukhov et al. 2009; Shulyak et al. 2009; Pandey et al. 2011).

Recently interferometry has been successfully applied to CP stars resulting in first estimate of the radii of three stars: α Cir (HD 128898, Bruntt et al. 2008), β CrB (HD 137909, Bruntt et al. 2010), and γ Equ (HD 201601, Perraut et al. 2011). No doubt interferometry is a powerful technique with a great advantage of providing model independent estimates of stellar sizes, its current world-wide facilities, unfortunately, are limited to only bright stars.

Send offprint requests to: D. Shulyak,
e-mail: denis.shulyak@gmail.com

In this work we apply a self-consistent atmospheric analysis to three well-known magnetic CP stars: β CrB (HD 137909), γ Equ (HD 201601), and 33 Lib (HD 137949). Collecting available photometric, spectrophotometric, and spectroscopic observations we perform detailed abundance and stratification analysis of a number of chemical elements in the atmosphere of each star. The effective temperatures and gravities are found iteratively by comparing theoretical fits to all available observables. Using fluxes calculated consistently with model atmospheres, available stellar parallaxes, and observed fluxes calibrated to absolute units we derive stellar radii and compare them with interferometric results.

2. Observations

Our investigation is based mainly on the low-resolution calibrated to absolute units spectroscopic observations obtained by Space Telescope Imaging Spectrograph (STIS)¹ mounted at the Hubble Space Telescope. STIS provides wide wavelength coverage ($\lambda\lambda 1700 - 10\,200$) excellent for the accurate analysis of energy distributions of early type stars where both UV and visual fluxes are of high importance. Among our targets only 33 Lib was not observed with STIS. Nevertheless, medium-band spectro-photometric observations by Adelman et al. (1989) are available for all objects, as well as UV fluxes from the International Ultraviolet Explorer (IUE)². For 33 Lib and β CrB additional wide-band UV fluxes were taken from the TD1 space mission (Boksenberg et al. 1973; Thompson et al. 1978). In case of β CrB we also made use of spectro-photometric measurements of Alekseeva et al. (1996), Breger (1976), Komarov et al. (1995), and UV low-resolution fluxes from ASTRON space satellite (Boiarchuk 1986).

Note that CP stars are known to demonstrate photometric variability most of which is caused by inhomogeneous surface distribution of chemical elements. However, as can be seen from e.g. Shulyak et al. (2010a); Krtićka et al. (2012), the amplitude of this variability is rather small to influence the derived effective temperatures much. For instance, using the Adelman's spectrophotometric catalog we find that the relative characteristic correction to the effective temperatures due to flux variability is only a few tens of K's for all three target stars. Because of this, and also because the listed above datasets are not homogeneous in sense of observing times and number of observations performed, we used mean fluxes when possible. For instance, only phase averaged fluxes were used from Adelman's catalog and IUE data archive.

Chemical abundance and stratification analysis was based on high-resolution, high signal-to-noise-ratio spectra obtained with the UVES instrument (Dekker et al. 2000) at the ESO VLT. Observations of 33 Lib and β CrB were carried out in the context of the program 68.D-0254, and published by, e.g., Ryabchikova et al. (2008), while spectra of γ Equ were extracted from the ESO archive (program 76.D-0169). Spectra of all three stars were obtained using both dichroic modes thus covering wavelength interval from $\lambda 3030$ to $\lambda 10400$ with a few gaps. Spectral resolution is about 80 000, signal-to-noise ratio at $\lambda 5000$ is about 300–400. Detailed description of the data reduction is given by Ryabchikova et al. (2008) (33 Lib and β CrB) and by Cowley et al. (2007) (γ Equ). In addition, for 33 Lib and γ Equ we used the UVES slicer spectra covering the $\lambda\lambda 4960 - 6990$ region and providing a resolving power

of $\lambda/\Delta\lambda \approx 115\,000$. Time-resolved observation of these stars were obtained in the context of ESO programs 72.D-0138 and 077.D-0150 (e.g. Kurtz et al. 2006). We used average spectra constructed from the total of 111 and 178 short exposures for 33 Lib and γ Equ, respectively. Reduction of these data followed procedures described by Ryabchikova et al. (2007).

In the course of our analysis we found out that for the β CrB and γ Equ the H β line of the UVES spectra always require systematically different temperatures compared to the one derived from SED and other hydrogen lines. We attribute this to an issue of continuum normalization and made use of additional observations from different instruments. In particular, for β CrB we used spectroscopic data obtained at 2.6-m telescope mounted at CrAO (Crimean Astrophysical Observatory) (Savanov & Kochukhov 1998). For γ Equ we used medium resolution spectra ($R \approx 37\,000$) obtained with the echelle spectrograph GIRAFFE, mounted at the 1.9-m Radcliffe telescope of SAAO (South African Astronomical Observatory). The data reduction of the GIRAFFE spectra was based on Vienna automatic pipeline for echelle spectra processing described in Tsybal et al. (2003).

3. Basic methods

3.1. Model atmospheres

Our approach is based on the models and synthetic fluxes computed with the LLMODELS stellar model atmosphere code (Shulyak et al. 2004). The code can treat individual homogeneous and depth-dependent abundances, which is a key feature in our modelling. In addition, the effect of the magnetic field is fully accounted via detailed computations of the anomalous Zeeman splitting and polarised radiative transfer as described in Khan & Shulyak (2006a). In all calculations we adopted magnetic field vector to lay perpendicular to the normal of the stellar surface (see Khan & Shulyak 2006b, for more details). This makes LLMODELS a powerful tool for the modelling of the observed characteristics of magnetic CP stars. The model fluxes are computed on a fine frequency grid with the highest points density at the wavelengths occupying the region of maximum stellar flux. A total of about 600 000 frequency points are usually used, which provides necessary resolution for the accurate computation of photometric indices of broad- and narrow-band photometric systems. Line opacity coefficient is computed based on atomic parameters extracted from the VALD database (Piskunov et al. 1995; Kupka et al. 1999), which presently includes more than 6.6×10^7 atomic lines. Most of them come from the latest theoretical calculations performed by R. Kurucz³.

Because of their large overabundance in atmospheres of Ap stars, rare-earth elements (REE) play an important and sometimes even dominating role in the appearance of spectroscopic features (Mashonkina et al. 2009, 2005) and can also affect much the spectral energy distribution (Shulyak et al. 2010b). Here we used the same line lists of REE elements as presented in Shulyak et al. (2010b). The studies by Mashonkina et al. (2009, 2005) demonstrated that the line formation of Pr and Nd can strongly deviate from the local thermodynamic equilibrium (LTE) with the doubly ionised lines of these elements are unusually strong due to combined effects of stratification of these elements and departures from LTE (known among spectroscopists as “REE anomaly”). However, a precise NLTE analysis is beyond the scope of this paper and currently could not be directly

¹ <http://www.stsci.edu/hst/stis>

² <http://archive.stsci.edu/iue/>

³ <http://kurucz.harvard.edu>

coupled to a model atmosphere calculation. Therefore, we followed the approach outlined in Shulyak et al. (2009) where the authors used a simplified treatment of the REE NLTE opacity by reducing the oscillator strengths for the singly ionised REE lines by the corresponding LTE abundance difference while using the abundances derived from second ions as an input for model atmosphere calculations (or vice versa). Applying this line scaling procedure allowed us to mimic the line strengths correspond to the NLTE ionization equilibrium abundance for each REE.

3.2. Abundance and stratification analysis

Initial homogeneous abundances for model calculations were taken from the papers by Ryabchikova et al. (2004) (33 Lib and β CrB) and by Ryabchikova et al. (1997) for γ Equ. These abundances were slightly corrected with synthetic spectral synthesis taking into account rather large magnetic fields of the program stars. Spectrum synthesis was performed by the magnetic synthesis code SYNTMAG (see Kochukhov 2007) using extraction of the atomic parameters and Landé-factors from the VALD database. To make abundance analysis of magnetic stars more efficient, we used equivalent width method with the newly developed code WIDSYN. This program provides an interface to the SYNTMAG code and allows to derive abundances using theoretical equivalent widths obtained from the full polarised radiative transfer spectrum synthesis. This improved equivalent width method greatly accelerates abundance analysis without sacrificing accuracy.

The stratification of chemical elements was modelled employing the DDAFrr IDL based automatic procedure which finds chemical abundance gradients from the observed spectra (see Kochukhov 2007). In this routine, the vertical abundance distribution of an element is described with the four parameters: chemical abundance in the upper atmosphere, abundance in deep layers, the vertical position of abundance step and the width of the transition region where chemical abundance changes between the two values. All four parameters can be modified simultaneously with the least-squares fitting procedure and based on observations of unlimited number of spectral regions. This procedure was successfully employed by a number of element stratification studies (e.g., Ryabchikova et al. 2005; Kochukhov et al. 2009; Shulyak et al. 2009; Pandey et al. 2011).

For Pr and Nd in γ Equ, we performed a NLTE stratification analysis as described in Mashonkina et al. (2005, 2009) using a trial-and-error method and the observed equivalent widths of the lines of the first and second ions. In NLTE calculations magnetic field effects were roughly approximated by pseudomicroturbulent velocity individual for each line. Such an analysis is applicable only for stars with small or moderate magnetic fields, e.g. for HD 24712, γ Equ (Mashonkina et al. 2005, 2009).

3.3. Determination of fundamental parameters

We follow the basic steps of the iterative procedure of atmospheric parameters determination outlined in, e.g., Shulyak et al. (2009). Briefly, this procedure consists of repeated steps of stratification and abundance analysis that provide an input for the calculations of model atmosphere until atmospheric parameters (T_{eff} , $\log(g)$, etc.) converge and theoretical observables (energy distribution, profiles of hydrogen lines, etc.) fit observations. Thus, the derived abundance pattern is consistent with the physical parameters of the final stellar atmosphere.

We used low resolution spectroscopic and/or spectrophotometric data calibrated to absolute units and available stellar parallaxes to derive radii of investigated stars. Fitting the full energy spectrum makes it possible to find reliable values for the atmospheric $\log(g)$ by matching the amplitudes of Balmer jump, which is very difficult or even impossible to do when only spectroscopic indicators or photometric indices are used. The fit to observed energy distributions is carried out on each iteration of abundance analysis using a grid of model atmospheres computed for a set of $[T_{\text{eff}}, \log(g)]$ values. The radii of the star is found by minimising the deviations between observed and predicted absolutely calibrated fluxes.

However, one important uncertainty remains in this analysis. As follows from the computations of atomic diffusion, helium always sinks in subphotospheric layers of A-F stars (Michaud et al. 1979). The same He depletion is found also by the diffusion models of the optically thin layers (Leblanc & Monin 2004), suggesting that the atmospheres of CP stars of spectral types A-F may well be He-deficient. No suitable diagnostic He lines are available for cool Ap stars to verify this conclusion observationally. The question whether or not helium is indeed removed from the atmosphere is of particular importance because this may noticeably change molecular weight and T-P stratification of He-weak models in deep layers where temperatures become high enough for He to contribute to the total opacity coefficient. Having no clues about true He stratification, we will thus consider an additional case of He-weak atmosphere with adopted He abundance of $[\text{He}/\text{H}] = -4$ (decreasing He abundance below this value has only marginal or no effect).

4. Results

In this section we present results of the parameter determinations for individual Ap stars, which are combined altogether in Table 1. For completeness, this table also lists our previous results derived for a few additional CP stars using the same analysis methodology. We also find that, with a few exceptions, the application of realistic model atmospheres did not result in a significant change of the mean element abundance estimates with respect to the studies cited above. Therefore, in the following we focus on the analysis of the vertical abundance profiles.

4.1. β CrB (HD 137909)

Among the three targets, β CrB is probably the most studied one. A number of independent spectrophotometric observations of energy distributions make it possible to test predictions of atmospheric models as well as estimate uncertainties of derived fundamental parameters in great detail. Furthermore, β CrB is known to be a binary system with orbital elements presented by Tokovinin (1984) and North et al. (1998). More recently Bruntt et al. (2010) carried out interferometric observations of the system which resulted in the first model-independent determination of the radii of primary (A) and secondary (B) components: $R(A) = 2.63 \pm 0.09 R_{\odot}$, $R(B) = 1.56 \pm 0.07 R_{\odot}$. Note, however, that authors still used scaled-solar models computed with ATLAS9 model atmosphere code (Kurucz 1992, 1993) to predict bolometric flux of the system and thus to derive effective temperatures for both components. This was necessary because all modern flux data always contain the combined light of the two components. This is also true for the STIS observation which was done with the 0.2'' slit width on 25 Aug 2003 when the visible separation between system components was $r < 0.1''$. Effective temperatures were found to be $T_{\text{eff}}(A) = 7980 \pm 180 \text{ K}$

and $T_{\text{eff}}(B) = 6750 \pm 230 \text{ K}$ respectively. The secondary component thus provides an important $\approx 18\%$ contribution to the bolometric flux of the system and thus has been taken into account in our SED fitting procedure.

Available spectra of β CrB made it possible to analyse stratification of five chemical elements: Mg, Si, Ca, Cr, and Fe, using from 8 to 23 neutral and singly-ionised lines per element. We did not perform NLTE Pr-Nd stratification analysis because of rather strong magnetic field and an absence of significant Pr-Nd anomaly (Ryabchikova et al. 2004) which is a manifestation of the rare-earth stratification. Starting from the $T_{\text{eff}} = 8000 \text{ K}$, $\log(g) = 4.3$ homogeneous abundance model and abundances presented in Ryabchikova et al. (2004), the atmospheric parameters was iterated to match the observed SED and profiles of hydrogen lines. All model atmospheres were computed with $\langle B_s \rangle = 5.4 \text{ kG}$ surface magnetic field (Ryabchikova et al. 2008). The best fitted parameter of the primary fall in the range $8000 < T_{\text{eff}}(A) < 8050 \text{ K}$, $3.9 < \log(g)(A) < 4.0$ and the respective fits to the SED and hydrogen lines are shown on Figs 1 and 2. Generally, the T_{eff} of the star is constrained by the slope of the Paschen continuum and hydrogen lines, while the $\log(g)$ is best controlled by the amplitude of the Balmer jump. We find that the contribution of the β CrB-B is crucial for the Paschen continuum and IR region, and ignoring it we were not able to obtain a consistent fit to SED and H-lines with any set of atmospheric parameters.

From Fig. 1 it is clear that there is a systematic difference between space and ground-based observations. Both STIS, IUE, TD1, and ASTRON data agree very well in UV region below $\lambda 2900$. At the same time, STIS provides less flux in visual and NIR than all ground-based photometric and spectrophotometric observations, which in turn agree fairly well with each other, with the exception of NIR (where some deviation can be seen, especially in the case of data from the Odessa catalog) and $\lambda\lambda 3800 - 5000$ region. Most likely this is due to different calibration methods applied to the observed data and its hard to give a preference to any of these datasets. Because STIS provides most homogeneous set of observations covering wide wavelength range from UV to NIR, we used it as a reference in the model fitting process.

Two problems still remain. First, none of the models can reasonably fit UV spectrum of the star below $\lambda 2500$. The secondary component is too faint to influence the combined flux in this spectral region. Because all UV data agree well with each other, we are inclined to conclude that this discrepancy between theoretical and observed fluxes is due to missing opacity in our models. The second problem arises from the fit to H-lines. Only $H\alpha$ and $H\beta$ are fit satisfactory. The computed profiles of $H\gamma$ are always wider than the observed ones even for He-weak model with lower $T_{\text{eff}} = 8050 \text{ K}$ that demonstrate somewhat better agreement for these two particular lines and worse for $H\alpha$. Increasing T_{eff} of the secondary within the limits given by Bruntt et al. (2010) one can obtain a slightly lower T_{eff} for the primary and thus narrower profiles of $H\gamma$ respectively, but the fit to both NIR fluxes and particularly $H\alpha$ profile becomes then noticeably worse. By integrating STIS fluxes and theoretical fluxes of the $A = [8050, 4.0, 2.50 \pm 0.07]$, $B = [6750, 4.2, 1.56]$ model we estimated a corresponding uncertainty in the effective temperature due to a difference between observed and predicted fluxes to be $\Delta T_{\text{eff}} = 50 \text{ K}$. This means that the true T_{eff} of β CrB is probably slightly overestimated in our analysis. On the other hand, an uncertainty in He abundance results in a similar 50 K error and thus accounting for both these effects could lower a temperature

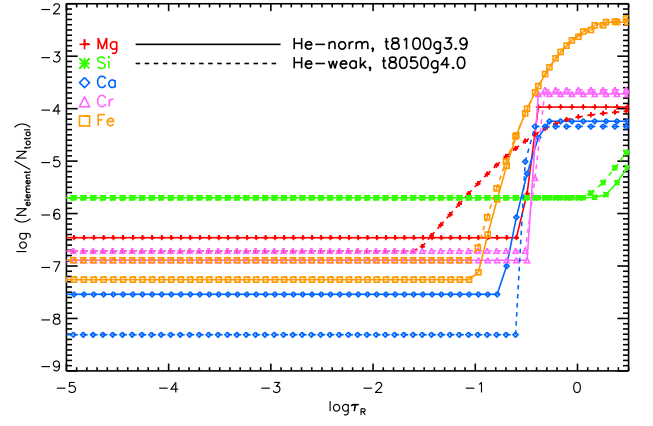


Fig. 3. Depth-dependent distribution profiles of chemical elements in the atmosphere of β CrB.

of the star by 100 K compared to the temperature derived in this study.

The final adopted parameters are (component = $[T_{\text{eff}}(\text{K}), \log(g)(\text{dex}), R(R_{\odot})]$): $A = [8050, 4.0, 2.50 \pm 0.07]$ for the He-weak model and $A = [8100, 3.9, 2.47 \pm 0.07]$ for the He-normal (e.g., with solar helium composition) model. The parameters of the secondary were taken from Bruntt et al. (2010): $B = [6750, 4.2, 1.56]$. We used the Hipparcos parallax of $\pi = 28.60 \pm 0.69 \text{ mas}$ from van Leeuwen (2007). The errors of the derived radii results from the stellar parallax uncertainty.

Using ground-based spectrophotometry led to a noticeable increase of the stellar radii. For instance, the fit to the data obtained by Breger (1976) require $A = [8050, 4.0, 2.70 \pm 0.07]$ for He-weak and $A = [8050, 3.8, 2.65 \pm 0.07]$ for He-norm models respectively.

The differences between STIS and ground-based observations correspond to the non-negligible difference in the derived stellar radii of $\Delta R \approx 0.2 R_{\odot}$. This reflects certain problems in the applied flux calibration procedures. But in spite of the vertical offset, the shape of SED's remains practically the same, therefore the effective temperatures derived from the two datasets are very similar.

Fig. 3 illustrates stratification profiles derived from the final He-norm and He-weak models. A substantial change in the position of the abundance jump is found for Mg for which He-norm model results in its narrowing and deeper position compared to He-weak model. Elements Ca and Fe demonstrated changes in the abundance amplitude in upper atmospheric layers, but we find that solution for Ca is quite uncertain in the highest layers with estimated errors of the order of $\pm 1 \text{ dex}$ or higher. Stratifications of Si and Cr stay almost unchanged, with Si accumulating at much deeper photospheric layers than what was found for other elements. Note that the changes in stratification profiles observed on Fig. 3 are due to combined effect of decreasing He content and T_{eff} by 50 K , i.e. not entirely due to He content. The effect of decreasing He abundance manifests itself in the increased $\log(g)$ by 0.1 dex needed to fit the SED of the star. Thus, accounting for a possible peculiar He content does have a well determined effect on the stellar parameter determination and we suggest to compute models with strongly deficient He content (i.e. in the same way it is done in this research) when analysing cool CP stars where true He abundance cannot be derived spectroscopically.

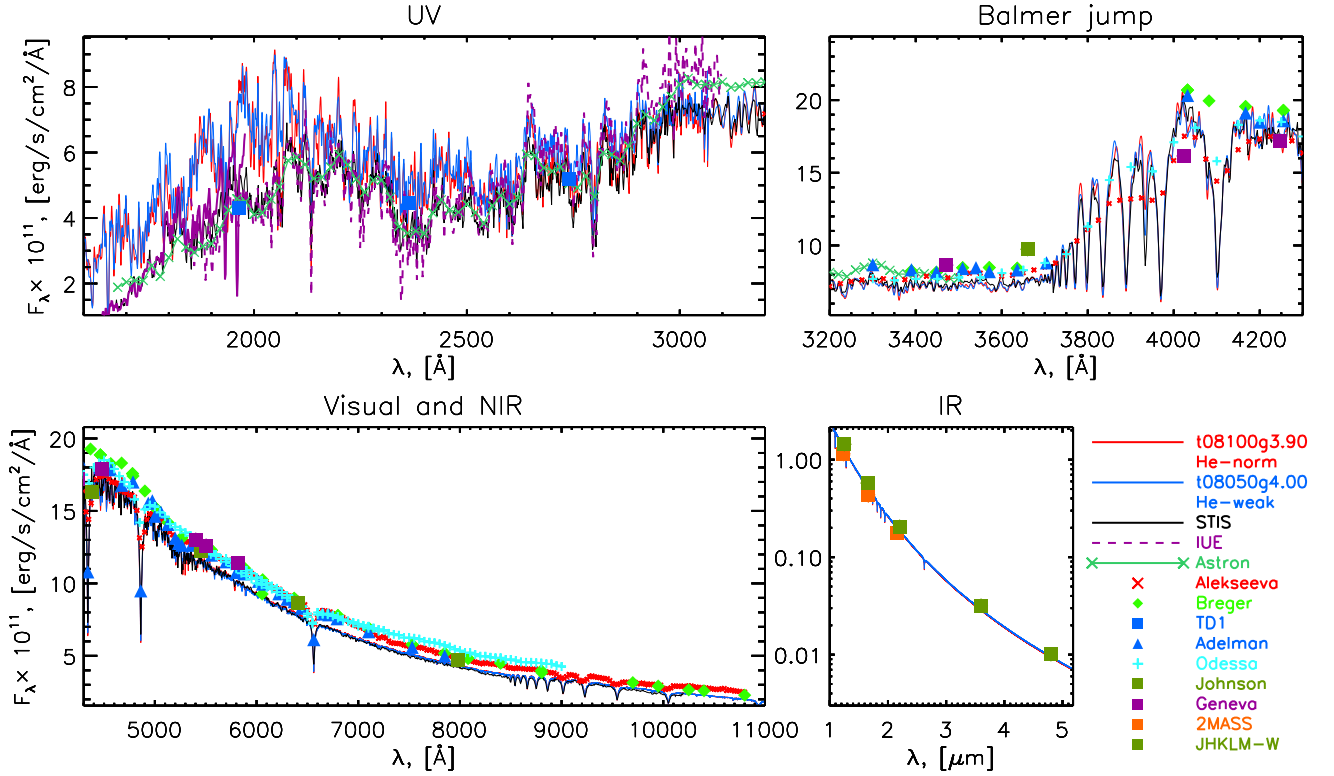


Fig. 1. Observed and predicted energy distributions of β CrB for two best fitted models with solar and depleted helium contents.

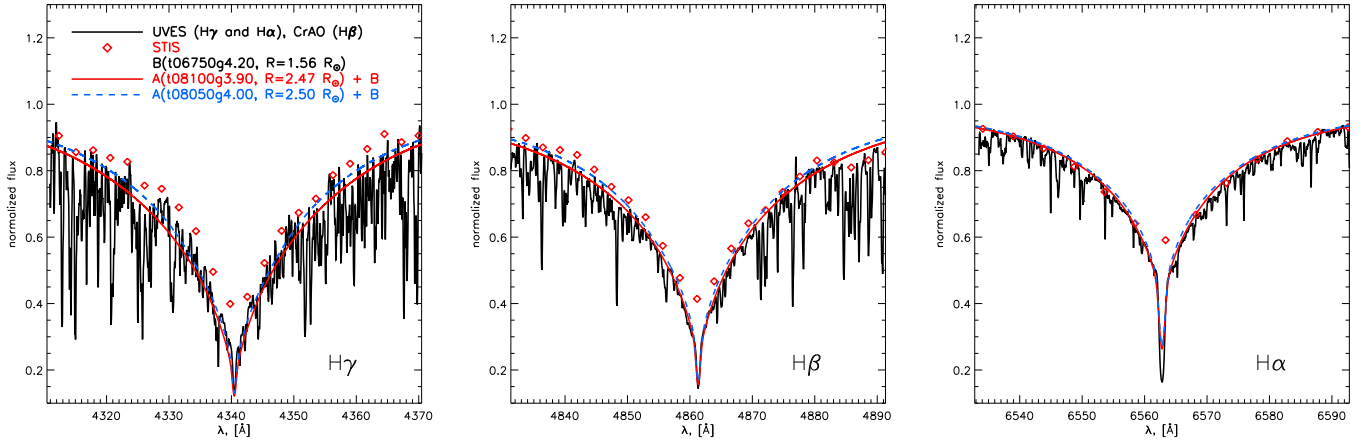


Fig. 2. Observed and predicted profiles of hydrogen lines of β CrB. Full line – He norm model; dashed line – He-weak model.

4.2. γ Equ (HD 201601)

γ Equ is another well known roAp star with rich spectrophotometric dataset available. Similar to β CrB, recent interferometric observations by Perraut et al. (2011) provided a radius of the star $R = 2.20 \pm 0.12 R_{\odot}$. γ Equ is also a binary system (see Fabricius et al. 2002) with γ Equ-B having much cooler temperature ($T_{\text{eff}}(B) = [4570, 4833]$ K) and thus smaller radius than β CrB-B, which then translated to the contribution of about 6% to the total flux of the system (Perraut et al. 2011). The authors also estimated the effective temperature of the system $T_{\text{eff}}(A + B) = 7364 \pm 235$ K, and thus $T_{\text{eff}}(A) = 7253$ K. This is much cooler than the temperature of $T_{\text{eff}} = 7700$ K adopted for γ Equ in the latest detailed spectroscopic study by Ryabchikova et al. (2002).

Due to extremely sharp spectral lines and weaker magnetic field which minimize the blending effects, γ Equ provides a possibility to perform a stratification analysis for 18 chemical elements: Na, Mg, Si, Ca, Sc, Ti, V, Cr, Mn, Fe, Co, Ni, Sr, Y, Zr, Ba, Pr, Nd. This represents the most complete empirical study of element diffusion in an atmosphere of a single star to date. Starting from the initial model with $T_{\text{eff}} = 7700$ K, $\log(g) = 4.2$ from Ryabchikova et al. (1997), we iterated stratification analysis and model atmosphere calculations until a minimal deviation between observed spectrophotometric observations and model fluxes was obtained. The surface magnetic field introduced in model atmosphere computations was $\langle B_s \rangle = 4$ kG. In Sc, V, Mn, Co stratification calculations laboratory data for hyperfine structure (hfs) were taken into account. They were extracted from the following

papers: Villemoes et al. (1992) (Sc II), Armstrong et al. (2011) (V II), Blackwell-Whitehead et al. (2005) (Mn I), Holt et al. (1999) (Mn II), Pickering (1996) (Co I), Bergemann et al. (2010) (Co II). Hyperfine structure for Pr II was also included in the Pr stratification analysis (see Mashonkina et al. 2009) with the *hfs*-constants from Ginibre (1989). In case of He-norm setting we find that models with $A = [7600, 4.0, 2.04 \pm 0.05]$, $B = [4500 - 4750, 4.5, 0.65 - 0.70]$ provide the best fit to the observed SED applying parallax $\pi = 27.55 \pm 0.62$ mas from van Leeuwen (2007). Assuming $B = [5000, 4.5, 0.80]$ results in a higher temperature of the primary $A = [7700, 4.0, 1.95 \pm 0.05]$. To fit the Balmer lines however, a lower effective temperatures of about $T_{\text{eff}} = 7300$ K is needed. Therefore, to maintain a satisfactory fit to both Balmer lines and SED a slightly cooler $A = [7550, 4.0, 2.07 \pm 0.05]$ was chosen. We note that formally model with $\log(g) = 3.8$ provides a better fit to SED ($\chi^2 = 1.19$) than the model with $\log(g) = 4.0$ ($\chi^2 = 1.40$) with a difference visible at the Balmer jump region (top right plot of Fig. 4). But the $\log(g) = 3.8$ then results in too small mass of the star, $M = 0.98 M_{\odot}$, which is unreasonable for a main sequence object with $T_{\text{eff}} = 7550$ K. No distinction could be made between these two $\log(g)$ from hydrogen line profiles as they are insensitive to the atmospheric gravity in this temperature range.

From the SED comparison presented on Fig. 4 it is seen that a good agreement between observations and model predictions is obtained for all represented spectral intervals from UV to IR. Ground based spectrophotometric data are also found to be consistent with the STIS observations, except observations obtained by Odessa research group which are systematically lower. The derived effective temperatures from the SED are reasonably close to that of Ryabchikova et al. (1997). This is because in the latter work the authors fitted observations of Adelman et al. (1989), which required $T_{\text{eff}} = 7700$ K to match the slope of the Paschen continuum.

Figure 5 compares the observed and predicted profiles of hydrogen lines. The normalisation of UVES data at the $H\beta$ line was found to suffer much from the data processing inaccuracies. Therefore we used observed profile taken with GIRAFFE instrument at SAAO. The normalisation of the STIS data in the same region is also not trivial but easier to perform due to its lower resolution and a wide wavelength coverage. On the other hand, $H\alpha$ line of STIS data is still satisfactory fitted with $T_{\text{eff}} = 7550$ K models, though UVES profile lays systematically higher and thus lower T_{eff} is needed to fit it.

The underabundance of He formally resulted in an increase of $\log(g)$ from 3.8 to 4.0 so that the He-weak model parameters are $A = [7550, 4.0, 2.06 \pm 0.05]$.

As follows from the results presented above, the most noticeably affected parameter is $\log(g)$ which undertook changes from 4.2 to 3.8 – 4.0 depending upon the helium abundance used. A value of $\log(g) = 4.2$ was used in Ryabchikova et al. (1997, 2002) to fit atomic lines using atmospheric models with a scaled solar abundances while in our analysis we used model atmospheres and fluxes computed with realistic abundances of the star. Finally, the use of STIS data allowed us to achieve a more detailed fit to the region of the Balmer jump, whose amplitude is very sensitive to the value of $\log(g)$.

The vertical distribution profiles of all 18 chemical elements derived with $T_{\text{eff}} = 7550$ K, $\log(g) = 3.8$, He-norm model are presented in Fig. 6. All but REE elements (i.e. Pr and Nd) are found to accumulate at layers just above the photosphere. For elements Ti and Ba stratification is not well constrained and probably is not present in the atmosphere of this star at all. A cloud of Pr and Nd is observed at high atmosphere and the abundance gra-

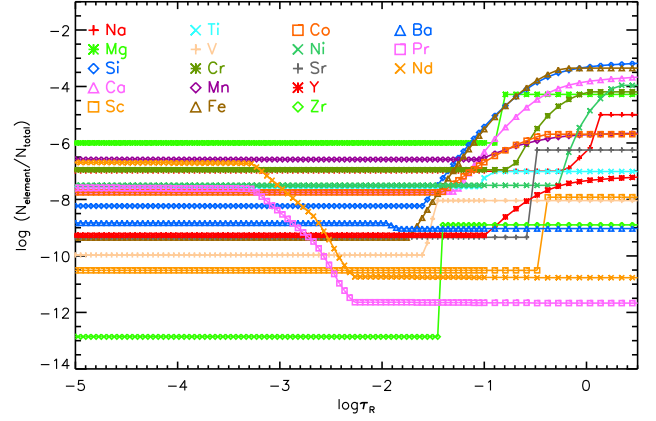


Fig. 6. Depth-dependent distribution profiles of chemical elements in the atmosphere of γ Equ.

dients of these elements, together with Fe and Si, are the largest among the studied elements.

4.3. 33 Lib (HD 137949)

33 Lib is the last target analysed in the present investigation. It is a bright roAp star with many references available regardless its spectroscopic and photometric properties. Unfortunately, no high resolution spectroscopic energy distribution similar to that provided by STIS is available, therefore a fit was done to the ground-based spectrophotometric data from Adelman et al. (1989). Our fitting began with $T_{\text{eff}} = 7550$ K, $\log(g) = 4.3$ model used by Ryabchikova et al. (2004, 2008). Stratification of Si, Fe, Ca, and Cr was derived and accounted in the model atmosphere calculations. Average abundances of the REE are higher in 33 Lib than in γ Equ by more than an order of magnitude. Stronger magnetic field of $\langle B_s \rangle = 5$ kG (Ryabchikova et al. 2008) together with high REE abundances result in extremely strong blending that prevents the proper choice of spectral lines for stratification study of other elements. It is also the reason why we could not perform NLTE stratification analysis of Pr and Nd based on equivalent widths and pseudomicroturbulence approximation of magnetic effects. It could be done only with the proper inclusion of the magnetic field in NLTE line formation code. Pr-Nd stratification is expected to be rather strong in 33 Lib because of the highest Pr-Nd anomaly observed in this star (Ryabchikova et al. 2004), however at present step we limit ourselves by taking into account the average observed REE anomalies.

The best-fit parameters are $[7400, 4.0, 2.13 \pm 0.13]$ for both He-norm and He-weak models. As shown on Fig. 7, also $[7300, 3.8, 2.19 \pm 0.13]$ and $[7500, 4.0, 2.06 \pm 0.13]$ models provide a reasonable fit, but with more pronounced deviations between the observed and predicted SEDs at short and long wavelengths.

Similar to other cases described above, for 33 Lib we also found it difficult to fit Balmer $H\alpha$ line with the model parameters required to fit the SED (see Fig. 8). A higher T_{eff} is required to fit observed profile of this line. On the other hand, $H\beta$ and $H\gamma$ lines are satisfactory fit with $T_{\text{eff}} = 7400$ K model.

The depth-dependent distribution of elements derived using the $[7400, 4.0]$ He-norm and He-weak models is shown on Fig. 9. As expected, in both cases the stratification profiles are

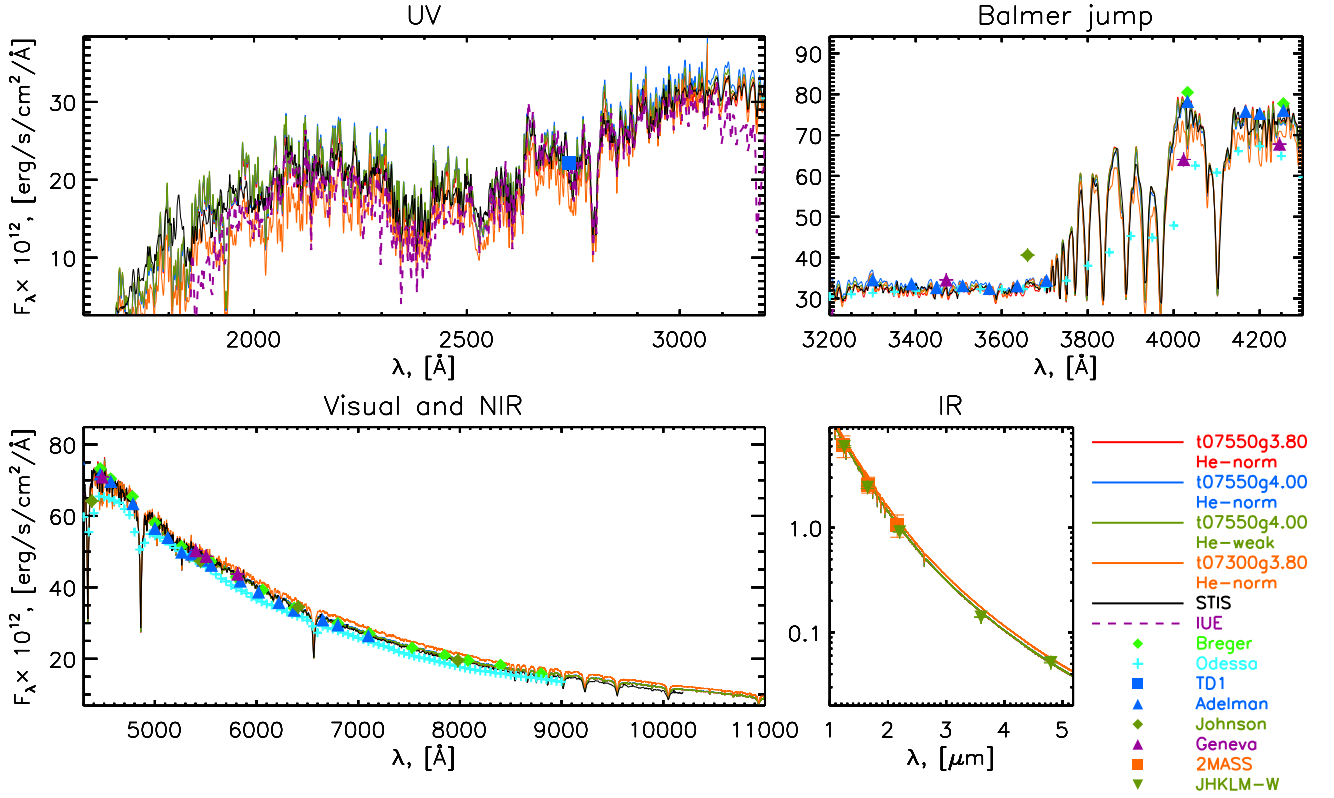


Fig. 4. Observed and predicted energy distributions of γ Equ for two best fitted models with solar and depleted helium contents.

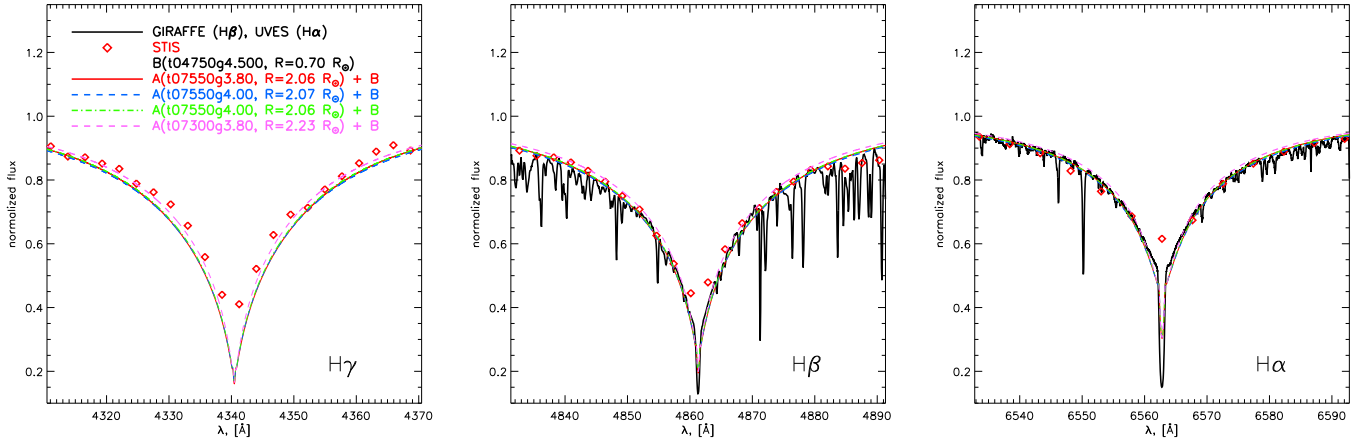


Fig. 5. Observed and predicted profiles of hydrogen lines of γ Equ. Dash-dotted lines correspond to He-weak model.

very similar, with large abundance jumps at deep atmospheric layers.

5. Discussion and conclusions

In an attempt to construct self-consistent models of Ap-star atmospheres, we performed a simultaneous model fit to a number of observed datasets, such as photometric wide-band fluxes, low- and middle-resolution spectrophotometric observations, and high-resolution spectra. Ideally, all of them must be fitted with a one single model atmosphere and abundance pattern. The results of the present investigation suggest that this is indeed possible to accomplish by applying a realistic chemical composition and appropriate model atmospheres that account for the peculiar nature of CP stars.

However, a few problems still exist. The most disturbing one is a systematic discrepancy between effective temperatures derived separately from SED and H-lines. In the case of β CrB only H α and H β are in agreement with SED, but H γ require lower T_{eff} . For 33 Lib the situation is opposite with H β and H γ being in agreement with T_{eff} derived from SED, but H α is clearly requiring a higher T_{eff} . A good match to SED, H α , and H β was obtained for γ Equ, though no high-resolution data was available for H γ line region. Since at least two out of three hydrogen lines are always in agreement with the atmospheric parameters derived from fitting the SED, it is likely that we face here the usual problem of continuum normalisation of the hydrogen lines in cross-dispersed echelle observations. Thus, one should always be cautious when determining atmospheric parameters solely based on the fit to hydrogen lines.

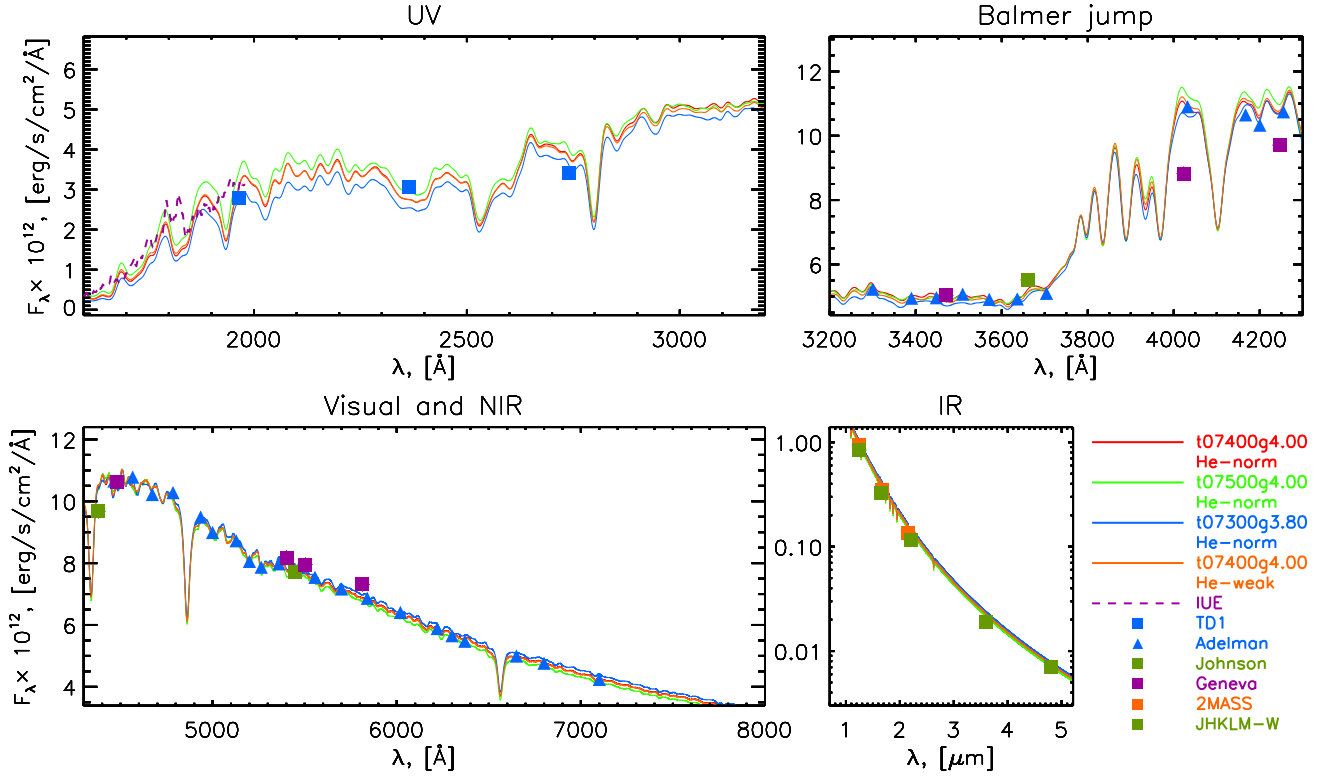


Fig. 7. Observed and predicted energy distributions of 33 Lib for two best fitted models with solar and depleted helium contents.

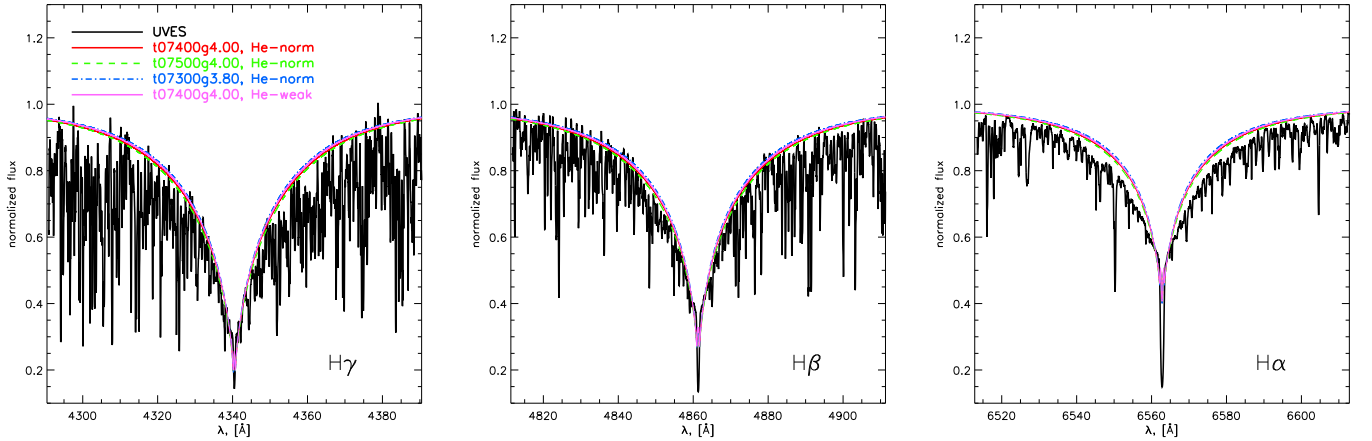


Fig. 8. Observed and predicted profiles of hydrogen lines of 33 Lib.

The abundance and stratification analysis was done using carefully selected spectral lines with accurately known transition parameters. Yet there seems to be a missing absorption in the models of β CrB in UV region blueward $\lambda 2500$ (see top left panel of Fig. 1). A secondary component is by far too faint and cool to influence the flux in that spectral region.

For β CrB we find a noticeable deviation between the space- and ground-based observations of the spectral energy distributions in the visual and NIR regions. A natural reason could be a discrepancy between different flux calibration schemes, which by default are more challenging in the case of ground-based observations. This deviation is seen as a vertical offset in the observed fluxes and do not affect the determination of T_{eff} (Fig. 1), but affects the radius estimate by about $0.2R_{\odot}$. This is quite a sen-

sible uncertainty and highlights once again the need of having accurately calibrated fluxes for stellar parameter determinations.

All previous spectroscopic studies resulted in the $\log(g)$ values that were substantially over-estimated, as shown by direct fits presented on Fig. 1, 4, and Fig. 7. Our values come mainly from the detailed fit to the amplitude and slope of the Balmer jump based on realistic model atmospheres. Previously only H-lines, photometric colors and/or low-resolution spectrophotometry by Adelman et al. (1989) were used in combination with scaled-solar metallicity models that did not account for individual abundances, magnetic fields, and improved REE opacity.

We find that possible He depletion of Ap-star atmospheres has a minor effect on determination of element distributions and $\log(g)$, at least for the hottest star, β CrB, considered here (see Fig. 3). Formally, an underabundance of He results in choosing

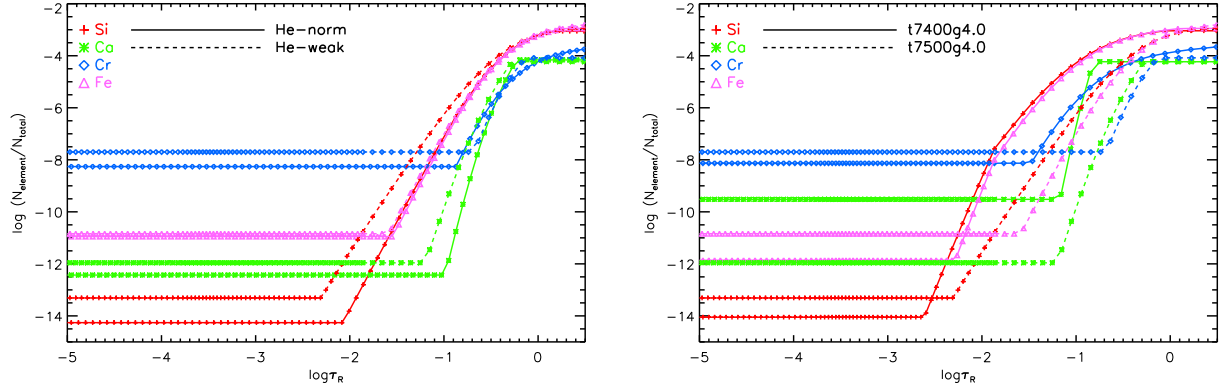


Fig. 9. Depth-dependent distribution profiles of chemical elements in the atmosphere of 33 Lib for He-norm and He-weak $T_{\text{eff}} = 7400$ K, $\log(g) = 4.0$ models (left panel) and two He-weak $T_{\text{eff}} = 7400$ K, $\log(g) = 4.0$ and $T_{\text{eff}} = 7500$ K, $\log(g) = 4.0$ models (right panel).

Table 1. Fundamental parameters of Ap stars.

Name	He-norm					He-weak					$R_{\text{inter}}^a, R_{\odot}$	$\langle B_s \rangle, \text{kG}$
	T_{eff}, K	$\log(g)$	R, R_{\odot}	L, L_{\odot}	M, M_{\odot}	T_{eff}, K	$\log(g)$	R, R_{\odot}	L, L_{\odot}	M, M_{\odot}		
HD 137909	8100	3.9	2.47 ± 0.07	23.69 ± 1.93	1.77 ± 0.51	8050	4.0	2.50 ± 0.07	23.67 ± 1.91	2.28 ± 0.65	2.63 ± 0.09^1	5.4
HD 201601	7550	4.0	2.07 ± 0.05	12.56 ± 0.94	1.56 ± 0.44	7550	4.0	2.06 ± 0.05	12.44 ± 0.93	1.55 ± 0.43	2.20 ± 0.12^2	4.0
HD 137949	7400	4.0	2.13 ± 0.13	12.27 ± 1.83	1.66 ± 0.58	7400	4.0	2.13 ± 0.13	12.27 ± 1.83	1.66 ± 0.58		5.0
HD 24712 ³	7250	4.1	1.77 ± 0.04	7.81 ± 0.57	1.44 ± 0.40							3.1
HD 101065 ⁴	6400	4.2	1.98 ± 0.03	5.92 ± 0.37	2.27 ± 0.59							2.3
HD 103498 ⁵	9300	3.5	4.56 ± 0.77	140.28 ± 50.39	2.40 ± 1.36							
	9500	3.6	4.39 ± 0.75	141.57 ± 51.35	2.80 ± 1.60							
HD 128898 ⁶	7500	4.1	1.94 ± 0.004	10.74 ± 0.33	1.73 ± 0.41						1.967 ± 0.066^7	~ 2.0

The error bars of M and R are average errors computed taking into account parallax uncertainty and additionally assuming errors of $\Delta T_{\text{eff}} = 50$ K and $\Delta \log(g) = 0.1$ dex. Larger errors found for HD 103498 result from a large parallax uncertainty.

^a Radius derived by means of interferometry.

¹ Bruntt et al. (2010); ² Perraut et al. (2011); ³ Shulyak et al. (2009); ⁴ Shulyak et al. (2010b); ⁵ Pandey et al. (2011); ⁶ Kochukhov et al. (2009);

⁷ Bruntt et al. (2008)

a slightly higher $\log(g)$ by about 0.1 dex and a cooler T_{eff} by ≈ 50 K. This change is small and well within the error bars of our fitting procedure. The choice of temperature has a somewhat stronger or at least a comparable impact on the derived stratification profiles of chemical elements, as can be seen from the example of 33 Lib illustrated on left and right panels of Fig. 9. In particular, a change of $\Delta T_{\text{eff}} = 100$ K influences both positions and amplitudes of the abundance jumps. It is important to realise, however, that even if we are not absolutely precisely in deriving T_{eff} and know nothing about the real He content of the Ap-star atmospheres, the inferred element stratifications are still informative and stable. Additional uncertainties could result from particular limitations in our fitting procedure (e.g., step-like approximation of stratification profiles, a small number of spectral lines used, etc.) and thus the presented analysis can only provide a general picture of the element distributions in the atmospheres of investigated stars. Still, this is enough to reveal an accumulation of particular element at the lower or upper atmospheric layers, determine the amplitudes of abundance jumps and estimate uncertainties of the derived distributions due to assumed model parameters – questions we were mainly interested in.

Interferometry has recently brought an entirely new possibility to measure radii of main-sequence stars on model-independent and regular basis, though its modern instrumental capabilities are limited only to bright nearby stars. Our model-

based comparison of the observed and predicted spectral energy distributions led to a good agreement (within error bars) with interferometric estimates as summarised in Table 1. The table also includes calculated masses and luminosities from derived effective temperatures, radii, and gravities. The corresponding error bars were calculated using individual uncertainties of stellar parallaxes along with typical uncertainties of $\Delta T_{\text{eff}} = 50$ K and $\Delta \log(g) = 0.1$ dex associated with the fit of SEDs and hydrogen line profiles. Large error bars found for HD 103498 are entirely due to a large parallax uncertainty ($\pi = 3.37 \pm 0.56$ mas given by van Leeuwen (2007)).

Figure 10 shows positions of stars from Table 1 in the H-R diagram along with theoretical evolutionary tracks. This comparison allows to derive stellar masses and ages under a reasonable assumption about the bulk stellar metallicity. Our spectroscopically derived masses generally show a good agreement with the theoretical values predicted by evolutionary models within estimated error bars. The only exception is HD 101065 for which evolutionary models predict $M = 1.48 M_{\odot}$ while Shulyak et al. (2010b) estimated $2.27 \pm 0.59 M_{\odot}$. In this particular case, however, the derived $\log(g)$ was very sensitive to the assumed line opacity of REE elements that were found to affect model fluxes in the Balmer jump region in a dramatic way. Because of NLTE effects and possible incompleteness of REE line lists the published value of $\log(g) = 4.2$ derived from the fit to the ob-

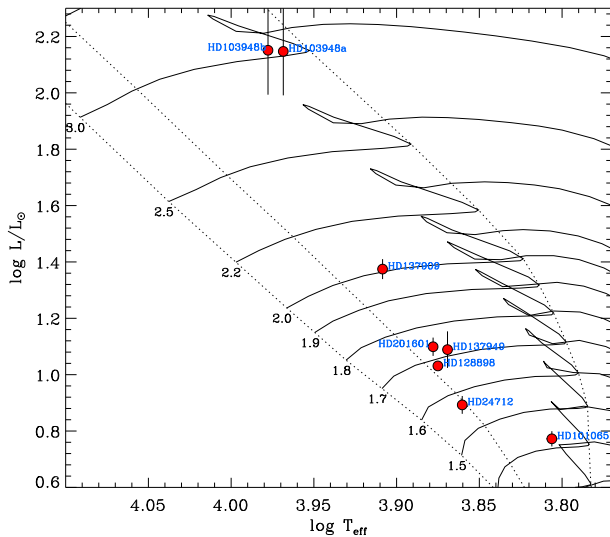


Fig. 10. Predicted location of Ap stars in the H-R diagram for the luminosity and temperature estimates from Table 1. Theoretical evolutionary tracks were adopted from Girardi et al. (2000) for the bulk metallicity of $Z = 0.018$. The dotted lines show ZAMS, 50% fractional main sequence age line and TAMS.

served SED could easily be overestimated and a somewhat lower $\log(g) = 4.0$ would give a consistent mass estimate.

Acknowledgements. We thank Dr. Igor Savanov for kindly providing us with H β spectrum of β CrB.

This work was supported by the following grants: Deutsche Forschungsgemeinschaft (DFG) Research Grant RE1664/7-1 to DS and Basic Research Program of the Russian Academy of Sciences “Nonstationary phenomena in the Universe” to TR. OK is a Royal Swedish Academy of Sciences Research Fellow supported by grants from the Knut and Alice Wallenberg Foundation and from the Swedish Research Council.

Some of the data presented in this paper were obtained from the Mikulski Archive for Space Telescopes (MAST). STScI is operated by the Association of Universities for Research in Astronomy, Inc., under NASA contract NAS5-26555. Support for MAST for non-HST data is provided by the NASA Office of Space Science via grant NNX09AF08G and by other grants and contracts.

We also acknowledge the use of electronic databases (VALD, SIMBAD, NASA’s ADS) and cluster facilities at Vienna Institute for Astronomy and Georg August University Göttingen.

References

- Adelman, S. J., Pyper, D. M., Shore, S. N., White, R. E., & Warren, W. H., Jr. 1989, *A&AS*, 81, 221
- Alekseeva, G. A., Arkharov, A. A., Galkin, V. D., et al. 1996, *Baltic Astronomy*, 5, 603
- Armstrong, N. M. R., Rosner, S. D., & Holt, R. A. 2011, *Phys. Scripta*, 84, 055301
- Armstrong, K. 2003, Master Thesis, Lund Observatory, Lund University, Sweden
- Bergemann, M., Pickering, J. C., & Gehren, T. 2010, *MNRAS*, 401, 1334
- Blackwell-Whitehead, R. J., Pickering, J. C., Pearse, O., & Nave, J. 2003, *ApJS*, 157, 402
- Boiarchuk, A. A. 1986, *Itogi Nauki i Tekhniki Seriya Astronomiya*, 31, 198
- Boksenberg, A., Evans, R. G., Fowler, R. G., et al. 1973, *MNRAS*, 163, 291
- Breger, M. 1976, *ApJS*, 32, 7
- Bruntt, H., Kervella, P., Mérand, A., et al. 2010, *A&A*, 512, A55
- Bruntt, H., North, J. R., Cunha, M., et al. 2008, *MNRAS*, 386, 2039
- Cowley, C. R., Hubrig, S., Castelli, F., Gonzalez, J. F., & Wolff, B. 2007, *MNRAS*, 377, 1579
- Dekker, H., D’Odorico, S., Kaufer, A., Delabre, B., & Kotzlowski, H. 2000, *proc. SPIE*, 4008, 534
- Fabricius, C., Høg, E., Makarov, V. V., et al. 2002, *A&A*, 384, 180
- Ginibre, A. 1989, *Phys. Scripta*, 39, 710
- Girardi, L., Bressan, A., Bertelli, G., & Chiosi, C. 2000, *A&AS*, 141, 371
- Holt, R. A., Scholl, T. J., & Rosner, S. D. 1999, *MNRAS*, 306, 107

- Khan, S. A., & Shulyak, D. V. 2006a, *A&A*, 448, 1153
- Khan, S. A., & Shulyak, D. V. 2006b, *A&A*, 454, 933
- Kochukhov, O., Shulyak, D., & Ryabchikova, T. 2009, *A&A*, 499, 85
- Kochukhov, O. 2007, in *Physics of Magnetic Stars*, eds. D. O. Kudryavtsev and I. I. Romanyuk, Nizhny Arkhyz., p. 109
- Komarov, N. S., Dragunova, A. V., Belik, S. I., et al. 1995, *Odessa Astronomical Publications*, 8, 3
- Krtićka, J., Mikulášek, Z., Lüftinger, T., et al. 2012, *A&A*, 537, A14
- Kupka, F., Piskunov, N., Ryabchikova, T. A., Stempels, H. C., & Weiss, W. W. 1999, *A&AS*, 138, 119
- Kurtz D. W., Elkin V. G., & Mathys G. 2006, *MNRAS*, 370, 1274
- Kurucz, R. L. 1992, *The Stellar Populations of Galaxies*, 149, 225
- Kurucz, R. 1993, *ATLAS9 Stellar Atmosphere Programs and 2 km/s grid*. Kurucz CD-ROM No. 13. Cambridge, Mass.: Smithsonian Astrophysical Observatory, 1993., 13
- Leblanc, F., & Monin, D. 2004, *The A-Star Puzzle*, 224, 193
- Mashonkina, L., Ryabchikova, T., Ryabtsev, A., & Kildiyarova, R. 2009, *A&A*, 495, 297
- Mashonkina, L., Ryabchikova, T., & Ryabtsev, A. 2005, *A&A*, 441, 309
- Michaud, G., Martel, A., Montmerle, T., et al. 1979, *ApJ*, 234, 206
- North, P., Carquillat, J.-M., Ginestet, N., Carrier, F., & Udry, S. 1998, *A&AS*, 130, 223
- Pandey, C. P., Shulyak, D. V., Ryabchikova, T., & Kochukhov, O. 2011, *MNRAS*, 417, 444
- Perraut, K., Brandão, I., Mourard, D., et al. 2011, *A&A*, 526, A89
- Pickering, J. C. 2006, *ApJS*, 107, 811
- Piskunov, N. E., Kupka, F., Ryabchikova, T. A., Weiss, W. W., & Jeffery, C. S. 1995, *A&AS*, 112, 525
- Ryabchikova, T., Kochukhov, O., & Bagnulo, S. 2008, *A&A*, 480, 811
- Ryabchikova, T., Sachkov, M., Kochukhov, O., Lyashko, D. 2007, *A&A*, 473, 907
- Ryabchikova, T., Leone, F., & Kochukhov, O. 2005, *A&A*, 438, 973
- Ryabchikova, T., Nesvacil, N., Weiss, W. W., Kochukhov, O., & Stütz, C. 2004, *A&A*, 423, 705
- Ryabchikova, T., Piskunov, N., Kochukhov, O., et al. 2002, *A&A*, 384, 545
- Ryabchikova, T. A., Adelman, S. J., Weiss, W. W., & Kuschnig, R. 1997, *A&A*, 322, 234
- Savanov, I. S., & Kochukhov, O. P. 1998, *Astronomy Letters*, 24, 516
- Shulyak, D., Krtićka, J., Mikulášek, Z., Kochukhov, O., Lüftinger, T. 2010a, *A&A*, 524, A66
- Shulyak, D., Ryabchikova, T., Kildiyarova, R., & Kochukhov, O. 2010b, *A&A*, 520, A88
- Shulyak, D., Ryabchikova, T., Mashonkina, L., & Kochukhov, O. 2009, *A&A*, 499, 879
- Shulyak, D., Tsymbal, V., Ryabchikova, T., Stütz Ch., & Weiss, W. W. 2004, *A&A*, 428, 993
- Thompson, G. I., Nandy, K., Jamar, C., et al. 1978, *Unknown*
- Tokovinin, A. A. 1984, *Pis’ma Astronomicheskii Zhurnal*, 10, 293
- Tsymbal, V., Lyashko, D., & Weiss, W. W. 2003, *Modelling of Stellar Atmospheres*, 210, 49P
- van Leeuwen, F. 2007, *A&A*, 474, 653
- Villemoes, P., Arnesen, A., F., Heijkskjöld, A., et al. 1992, *Phys. Scripta*, 46, 45